

Automatika

Journal for Control, Measurement, Electronics, Computing and Communications



ISSN: (Print) (Online) Journal homepage: www.tandfonline.com/journals/taut20

Design, analysis and comparison of switched reluctance motors for electric vehicle application

L. Ananda Padmanaban & P. Saravanan

To cite this article: L. Ananda Padmanaban & P. Saravanan (2023) Design, analysis and comparison of switched reluctance motors for electric vehicle application, *Automatika*, 64:2, 239-247, DOI: [10.1080/00051144.2022.2140388](https://doi.org/10.1080/00051144.2022.2140388)

To link to this article: <https://doi.org/10.1080/00051144.2022.2140388>



© 2022 The Author(s). Published by Informa UK Limited, trading as Taylor & Francis Group.



Published online: 06 Nov 2022.



Submit your article to this journal [↗](#)



Article views: 2212



View related articles [↗](#)



View Crossmark data [↗](#)



Citing articles: 3 View citing articles [↗](#)



Design, analysis and comparison of switched reluctance motors for electric vehicle application

L. Ananda Padmanaban  and P. Saravanan

Department of Electrical and Electronics Engineering, Sri Sivasubramaniya Nadar College of Engineering, Kalavakkam, Tamil Nadu, India

ABSTRACT

This paper presents the design, analysis and comparative study of three different configurations of Switched Reluctance Motor (SRM) suitable for In-wheel application in Electric Vehicles. C-core stator with dual rotor SRM, C-core stator with disk-type segmented rotor SRM and Dual gap inner segmented rotor SRM are designed and compared for the same stator/rotor pole, supply current, current density and outer diameter. The significant performance indices of an electric motor for an in-wheel application, such as torque ripple, torque per unit active weight and torque per unit active volume, are considered for analysis. 3D Finite Element Analysis (FEA) of the machines is performed using the software MagNet 7.5 due to the axial field distribution of the configurations. The best among the three configurations is fabricated and experimental results are presented.

ARTICLE HISTORY

Received 24 January 2022
Accepted 20 October 2022

KEYWORDS

Axial flux switched reluctance motor; electric vehicles; finite element analysis; in-wheel motors

1. Introduction

Electric Vehicles (EVs) are the need of the hour due to environmental issues and the depletion of fossil fuels across the world [1,2]. Many countries have planned to switch over to EVs shortly [3,4]. The range of EVs which was the major hurdle for the prevalent use of EVs has been overcome by the advent of battery technology and efficient drive systems. The conventional single-motor drive requires a reduction gear, transmission and mechanical differential which results in transmission losses. Transmission losses in EVs lead to lesser efficiency, lesser range, higher operating cost and more weight [4]. Multi-motor drive constituting motor inside the wheels eliminates the transmission system and its losses [5].

Permanent Magnet Machines (PMM) dominate in in-wheel EV applications due to their high-power density [4]. Depletion of rare earth magnetic resources and unstable magnet price pave way for alternate motor technology [6–8]. Switched Reluctance Motor (SRM) is inevitable due to their dominating advantages such as simpler construction, higher fault-tolerant capability, lower cost and magnet-free operation [9–11]. SRM has been in use for EV applications since 1838 [6].

In reference [12], a 3/2 Dual stator single rotor Axial Flux Switched Reluctance Motor (AFSRM) has been proposed. The stator and rotor poles are segmented and supported by an aluminium disc. The lamination of the stator and rotor poles is not addressed. The stator poles are 90° tilted “U” shape and the rotor is just a circular strip. The lamination of the rotor and stator poles

is highly complex. Accommodation of conductors in the stator is not simple and increases the axial length of the motor. The winding of stator coils is difficult. In reference [13], a four-phase, 8/6 pole dual stator single rotor AFSRM has been proposed. Dual stator configuration balances the axial force between the stator pole and rotor pole. The laminated structure of the rotor and stator cores is achieved by the strip winding technique. This reduces the core losses in the poles but not in the back iron. In reference [14], a four-phase, 8/6 pole segmented stator, dual rotor SRM has been proposed. The stator constitutes a segmented C-Core enabling easier winding. Larger slot space, simple structure and lesser rotor inertia are the notable features of the configuration. In reference [15], a five-phase, 15/12 pole pancake-shaped AFSRM has been proposed. The stator consists of a “C” type core and is isolated from each other magnetically. The rotor consists of segmented cubes embedded in an aluminium disc. The advantages are the absence of radial forces resulting in lower vibration and acoustic noise. The lamination of stator and rotor cores is simple. A higher number of phases result in higher switching losses and bulky converters. In reference [16], a three-phase, 12/8 pole-segmented AFSRM has been proposed. The segmented rotor increases torque output, simplifies fabrication and reduces acoustic noise and vibration. A dual rotor with a double-sided stator in between them balances axial forces between the stator and rotor pole. Toroidal-type stator winding makes winding difficult with no possibility of pre-formed coils. In reference [17], a

three-phase, 12/16 segmented AFSRM with rotor poles higher than the stator pole has been proposed. The structure also uses a dual rotor with a toroidal wound stator. The advantage of a higher number of rotor poles than the stator pole is the reduced axial length of the motor. In reference [18], a four-phase, 8/6 pole dual rotor with a single double-sided stator has been proposed. The stator windings on each side are independently controlled such that the excitation can be one or two at a time. Depending on the number of excitations the magnetic circuit and operation vary. In reference [19], to circumvent the difficult task of laminating the rotor and stator core of AFSRM Soft Magnetic Composite (SMC) materials are used. In reference [20], a single segmented rotor in between dual stators is investigated. The two stators are skewed by an angle with respect to the rotor to reduce torque ripple. Windings in the stator are simple concentric. In reference [21], a geometric modification of the rotor in reference [20] is done. The rotor poles on each side are displacement by an angle to reduce the torque ripple. In reference [22], a 12/8 pole segmented stator AFSRM has been proposed. The stator poles are “C” shaped and the rotor poles are simple rectangular bars. The configuration has one stator and one rotor leading to unbalanced axial forces between the rotor and stator poles. Most of the configurations available in the literature fall under the three configurations [14], [15] and [20] with minor changes in the geometry and flux path. Hence the comprehensive analysis of the three configurations will provide insight into all the other configurations.

- (1) Type I, C-core stator with dual rotor: The single stator is formed by multiple C-shaped segments. The two rotors are non-segmented and held together by the shaft (Figure 1).
- (2) Type II, C-core stator with a disc-type segmented rotor: This AFSRM consists of a single stator formed by C-shaped segments. The rotor is made up of ferromagnetic cubes embedded in a non-magnetic material (Figure 2).
- (3) Type III, Dual gap inner segmented rotor: In this configuration, the rotor has ferromagnetic rotor poles embedded in a non-magnetic disc and the two stators are non-segmented placed one on each side of the rotor disc (Figure 3).

Though all the machine suits the EV application, a comparative study of performance and feature would help in finding the best configuration among the three. The performance indicators chosen for comparison are torque ripple (T_r), torque per unit active weight (P_{AW}), torque per unit active volume (P_{AV}), copper loss (P_c), copper weight (W_c) and iron weight (W_i). The comparison is based on the results obtained from the numerical method using a 3-D Finite Element Analysis (FEA) software, MagNet 7.5. A prototype of the

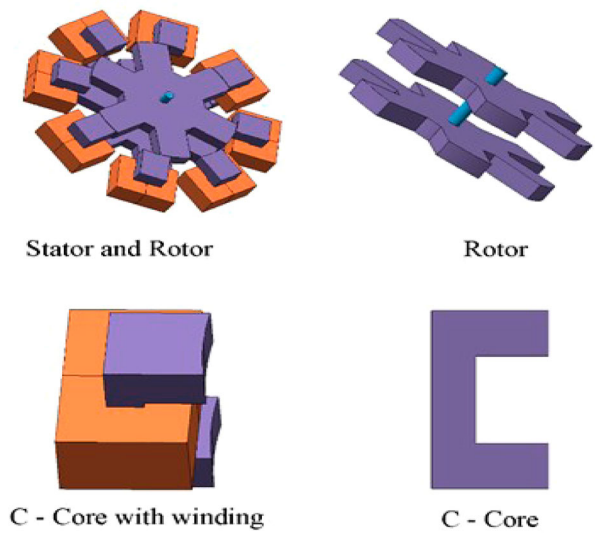


Figure 1. Type I, C-core stator with a dual rotor.

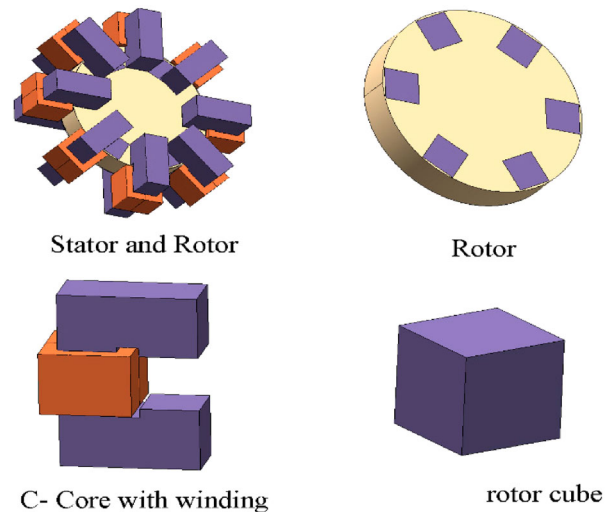


Figure 2. Type II, C-core stator with disk-type segmented rotor.

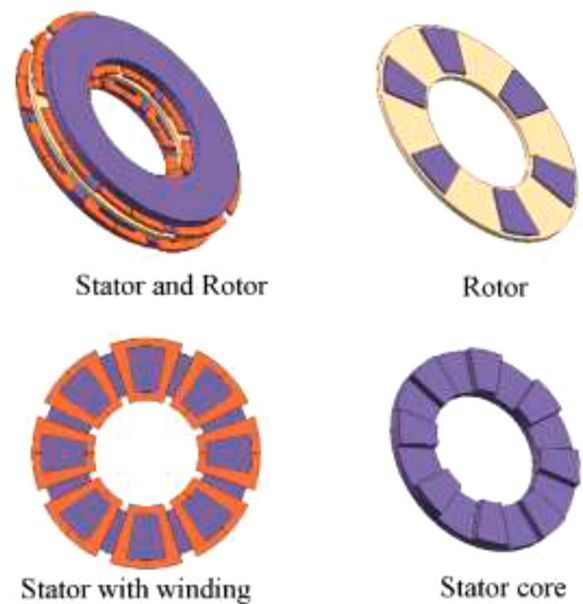


Figure 3. Type III, Dual gap inner segmented rotor.

best configuration among the three is fabricated and experimental results are presented.

2. Design of in-wheel motors

The in-wheel application of the motor features a diameter larger than its length. Volume restrictions demand high power density from in-wheel motors. To identify the best configuration among them, current, current density, outer diameter of stator, air gap and core material are held as common in the design process. The values of the above parameters are given in Table 1.

The output equation of AFSRM can be derived from the first principles of electromagnetics.

The voltage equation neglecting the stator resistance is

$$v = \frac{d\psi}{dt} \quad (1)$$

where flux linkage ψ , for current I and inductance L is

$$\psi = L \times I \quad (2)$$

For a stator pole arc of β_s radian, and motor speed of ω_m rad/s, the time taken t , to reach an aligned position from the unaligned position is

$$t = \frac{\beta_s}{\omega_m} \quad (3)$$

Using (2) and (3), the voltage

$$v = \frac{(L_a - L_u) \times I \times \omega_m}{\beta_s} \quad (4)$$

where L_a – aligned inductance; L_u – unaligned inductance

Rearranging (4)

$$v = \frac{\omega_m}{\beta_s} \times L_a \times I \times k_u \quad (5)$$

where

$$k_u = 1 - \frac{L_u}{L_a} \quad (6)$$

The flux linkage of the coil at an aligned position, in terms of turns per phase, N_{ph} and flux Φ in the stator pole, is

$$L_a \times I = \phi \times N_{ph} \quad (7)$$

The flux in the stator pole of area A_{sp} and flux density B is given as

$$\phi = B \times A_{sp} \quad (8)$$

Table 1. Common parameters of the motors designed.

Parameter	Symbol	Value
Current density (A/mm ²)	J	5.21
The outer diameter of the stator (mm)	D_o	254
No of stator poles	N_s	8
No of rotor poles	N_r	6
Air gap (mm)	Ag	0.5
Torque (Nm)	T	4.75
Core material	–	M-36 Steel

$$L_a \times I = B \times A_{sp} \times N_{ph} \quad (9)$$

$$v = \frac{\omega_m}{\beta_s} \times B \times A_{sp} \times N_{ph} \times k_u \quad (10)$$

Power developed P_d , in terms of voltage (v) and current (I) for “m” no of phases conducting simultaneously is,

$$P_d = k_e \times k_d \times v \times I \times m \quad (11)$$

where k_e – efficiency; k_d – duty cycle.

Using (10), in (11), the generalized power developed equation is

$$P_d = \frac{1}{\beta_s} \times k_e \times k_d \times k_u \times \omega_m \times N_{ph} \times I \times B \times A_{sp} \times m \quad (12)$$

Area of the stator pole of Type I is

$$A_{sp1} = \beta_s \times L_{sr} \times r_o \quad (13)$$

where L_{sr} – Length of stator pole; r_o – Outer radius of the rotor. The area of the stator pole of Type II is

$$A_{sp2} = \beta_s \times L_r \times r \quad (14)$$

where L_r – Length of rotor cube; r – Distance from the rotor cube to the shaft.

The area of the stator pole of Type II is

$$A_{sp3} = \frac{\beta_s}{8} \times (D_o^2 - D_i^2) \quad (15)$$

where D_o – The outer diameter of the stator pole; D_i – The Inner diameter of the stator pole. Substituting (13), (14) and (15) in (12), Equations (16), (17) and (18) represent the developed power of Type I, Type II and Type III, respectively.

$$P_d = K_e K_d K_u \omega_m N_{ph} I B L_{sr} r_o \quad (16)$$

$$P_d = K_e K_d K_u \omega_m N_{ph} I B L_r r \quad (17)$$

$$P_d = K_e K_d K_u \omega_m N_{ph} I B L_{sr} (D_o^2 - D_i^2) / 8 \quad (18)$$

3. Analysis of the chosen configurations

The complex part of the design of electrical machines is the estimation of magnetic flux distribution in the different parts of the machine and the corresponding flux density in each part. Analytical methods of finding the flux distribution by assuming the flux tubes are complex and less accurate for the axial field-distributed machines. Numerical methods, such as Finite Element Analysis, yield accurate results. The electromagnetic analysis of the three configurations is done with the help of the Finite Element Analysis software, MagNet 7.5.

3.1. Ratio of aligned inductance to unaligned inductance

From the power output equation, the power developed by the machine depends upon the factor K_u . Higher values of K_u require a ratio of aligned inductance (L_a) to unaligned inductance (L_u) to be high. The extent of the high-speed operation is dictated by the unaligned inductance and aligned inductance. Hence low values of inductances while maintaining a high ratio are required. Table 2 shows the values of inductance and factor K_u of each configuration. Type III configuration features higher values of K_u and lower values of L_a and L_u .

3.2. Flux density distribution

The preliminary analysis is the flux density distribution in different components of the machine to arrive compact design with less core loss. Maximum flux flows in the machine at an aligned position when rated current is supplied, as shown in Figures 4–6. Type III configuration has fewer flux densities in the areas such as stator pole, rotor pole and stator back iron than Type I and Type II which is an important aspect for core loss.

3.3. Current–flux linkage characteristics

The Current–Flux linkage characteristics are mandatory to determine the average torque analytically and for the design of controllers. The characteristics are shown in Figures 7–9. Type III configuration delivers more flux linkage than Type I and Type II for all values of current.

Table 2. Values of inductances and factor K_u .

Parameter	Type I	Type II	Type III
L_a (mH)	5.30	5.86	6.64
L_u (mH)	1.66	1.78	0.93
K_u	0.69	0.70	0.86

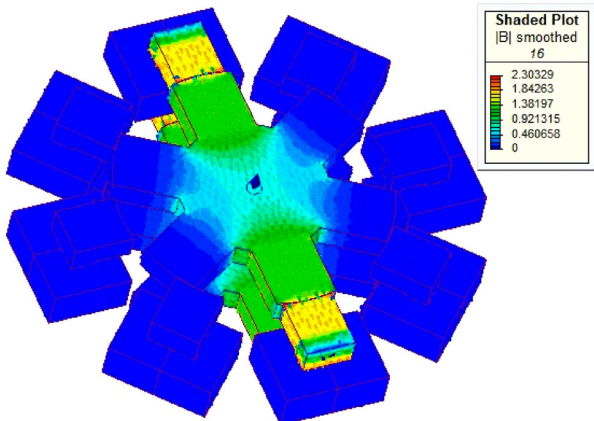


Figure 4. Flux density distribution of Type I.

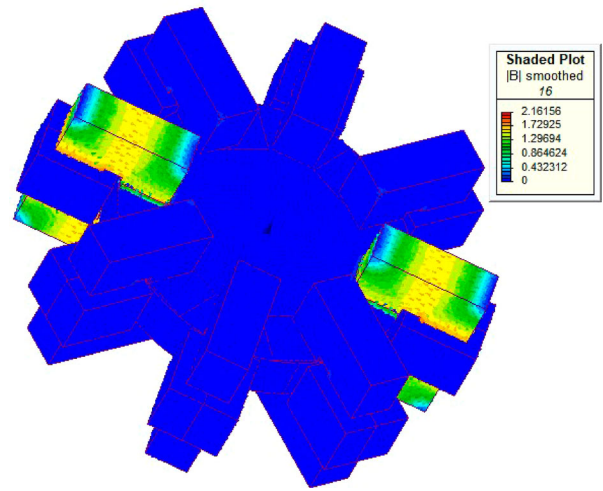


Figure 5. Flux density distribution of Type II.

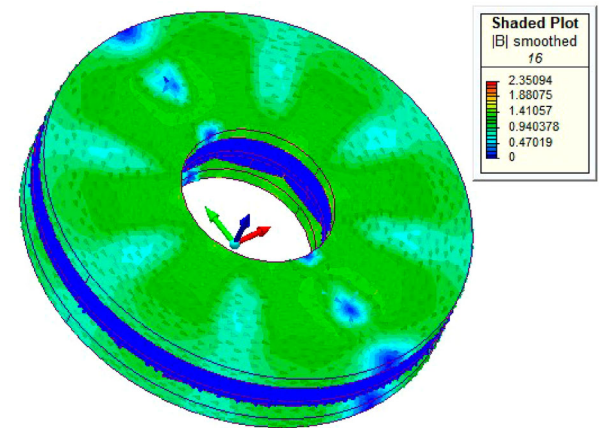


Figure 6. Flux density distribution of Type III.

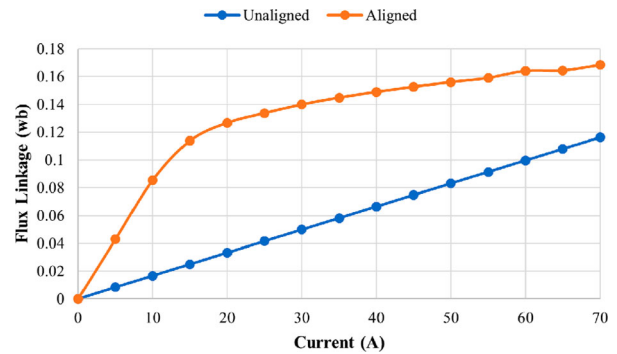


Figure 7. Current–Flux linkage characteristics of Type I.

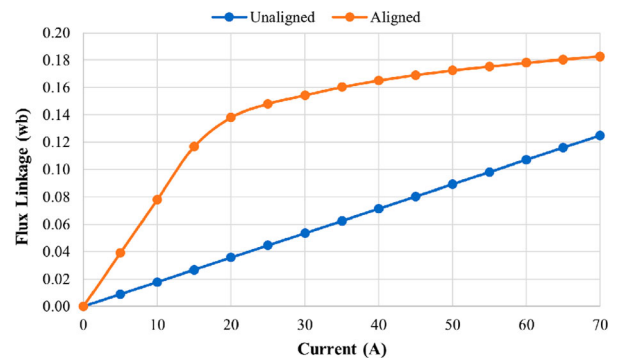


Figure 8. Current–Flux linkage characteristics of Type II.

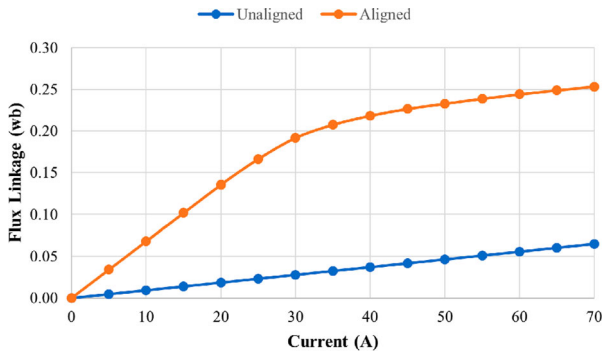


Figure 9. Current–Flux linkage characteristics of Type III.

3.4. Torque–rotor position characteristics

The static torque–rotor position characteristics are very essential in determining the average torque, torque ripple, peak torque and ideal turn-on–turn off the angle of each phase. For an 8/6 SRM the periodicity of this torque is 60° . Hence, it is sufficient to determine the torque for 60 different rotor positions starting from an unaligned position. The characteristics are shown in Figures 10–13. The torque ripple is the minimum for the Type III configuration.

3.5. Torque–current–rotor position characteristics

High torque per ampere should be achieved to have good efficiency, easy cooling and a lesser volume of the machine. In SRM the torque is proportional to the square of the current. The torque obtained at different

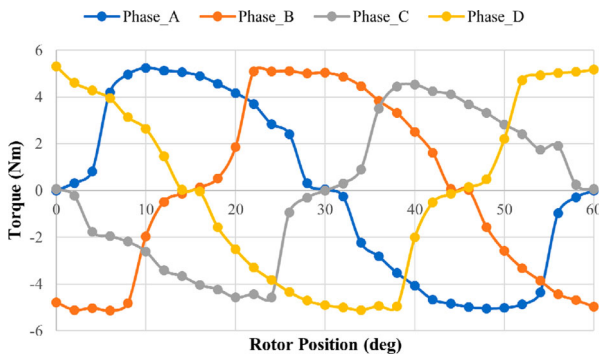


Figure 10. Torque–Rotor Position characteristics of Type I.

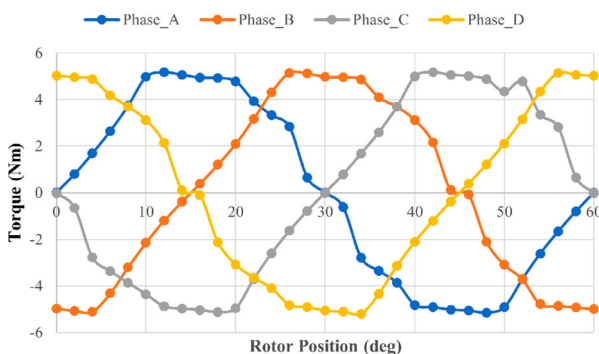


Figure 11. Torque–Rotor Position characteristics of Type II.

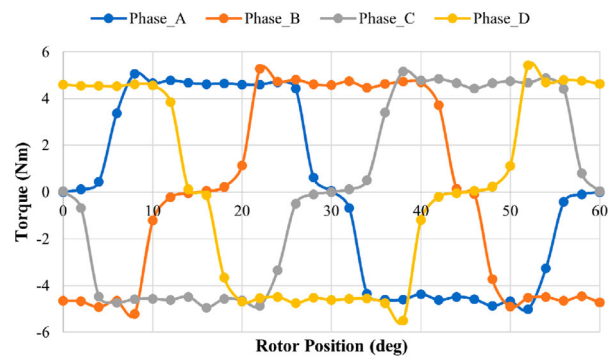


Figure 12. Torque–Rotor Position characteristics of Type III.

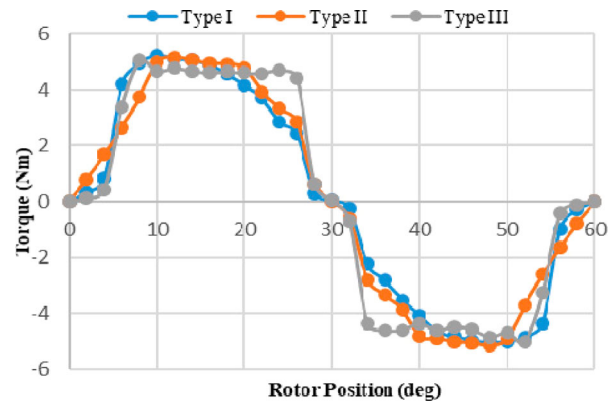


Figure 13. Torque–Rotor Position characteristics of Type I – III.

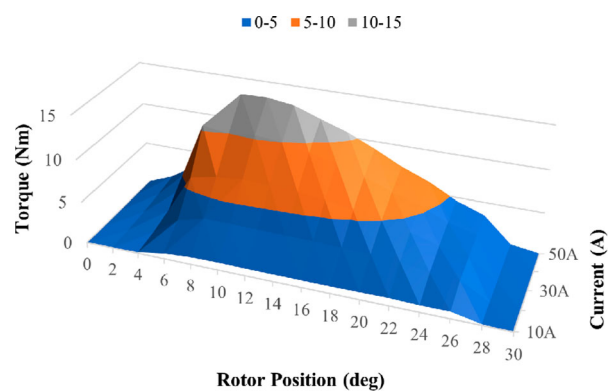


Figure 14. Torque–Current–Rotor Position characteristics of Type I.

positions of the rotor for a current of 10 A, 20 A, 30 A, 40 A and 50 A is shown in Figures 14–16. As the current increases, the torque output decreases due to the saturation of the machine. From the figure, it is evident that the Type III configuration delivers more torque at a higher current than the other two configurations.

4. Comparison of the three configurations

The three types of configurations are compared in terms of different performance parameters and features. Table 3 shows the values of each parameter for all three types of motors. No motor is superior in all aspects. Type I is superior in the aspects such as lower values of aligned

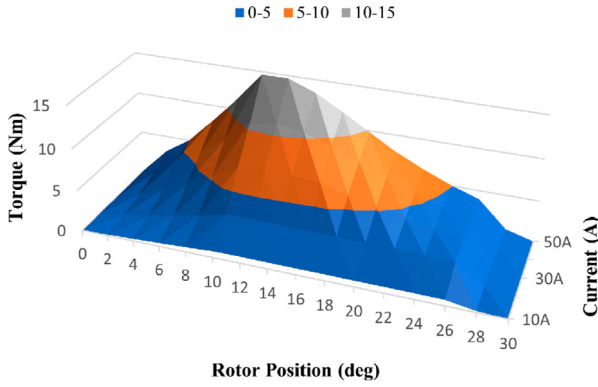


Figure 15. Torque–Current–Rotor Position characteristics of Type II.

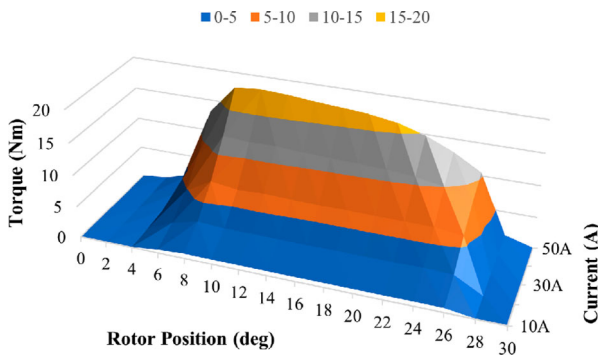


Figure 16. Torque–Current–Rotor Position characteristics of Type III.

Table 3. Performance indices of the three types of motor.

Parameter	Type I	Type II	Type III
L_a (mH)	5.30	5.86	6.64
L_u (mH)	1.66	1.78	0.93
L_a/L_u	3.19	3.29	7.15
T_r (%)	37.10	31.14	20.82
W_i (kg)	6.88	11.13	8.61
W_c (kg)	2.48	1.79	1.73
A_w (kg)	9.36	12.92	10.34
P_c (W)	76.98	52.60	55.18
T_{AW} (Nm/kg)	0.51	0.36	0.46
T_{AV} (kNm/m ³)	1.27	0.76	1.43

inductance (L_a), lower values of iron weight (W_i), lower values of active weight (A_w) and higher values of torque per unit active weight (T_{AW}). Type I is inferior in the aspects of lesser L_a/L_u ratio, higher torque ripple (T_r), higher copper weight (W_c) and higher copper loss (P_c). Type II is superior in lesser copper loss (P_c) and inferior in higher unaligned inductance (L_u), higher iron weight (W_i), higher active weight (A_w), lower torque per unit active weight (T_{AW}) and lower torque per unit active volume (T_{AV}). Type III is superior in lesser unaligned inductance (L_u), higher L_a/L_u ratio, lesser torque ripple (T_r), lesser copper weight (W_c) and higher torque per unit active volume (T_{AV}). Type III is inferior in higher aligned inductance (L_a). Each motor has superior features in a few aspects and inferior in other aspects.

4.1. Aligned inductance (L_a) and unaligned inductance (L_u)

High values of aligned and unaligned inductances result in high rise time and fall time of current resulting in a limited speed of operation of the motor. L_a and L_u are obtained from the flux linkage of the coil corresponding to the rated current when the rotor is at an aligned and unaligned position, respectively. Type I has the lowest aligned inductance and Type III has the lowest unaligned inductance.

$$L_a = \frac{\psi_{\text{aligned}}}{I_{\text{rated}}} \quad (19)$$

$$L_u = \frac{\psi_{\text{unaligned}}}{I_{\text{rated}}} \quad (20)$$

where L_a – aligned inductance; L_u – unaligned inductance; ψ_{aligned} – flux linkage at the aligned position; $\psi_{\text{unaligned}}$ – flux linkage at the unaligned position; I_{rated} – rated current.

4.2. Ratio of L_a to L_u (L_a/L_u)

From the torque equation, it is evident that the torque output and the power output of SRM depend on the ratio of L_a to L_u and not on the values of L_a and L_u . Type III has the highest ratio of L_a to L_u .

4.3. Torque ripple (T_r)

No machine is free from Torque ripple and SRM produces high torque ripple compared to other types of machines. The torque ripple produced by Type III motor is lesser than the other two types for a current of 25 A.

$$T_r(\%) = \frac{T_{\text{max}} - T_{\text{min}}}{T_{\text{avg}}} \times 100 \quad (21)$$

where T_{max} – Maximum torque in Nm; T_{min} – Minimum torque in Nm; T_{avg} – Average torque in Nm.

4.4. Torque per unit active weight (T_{AW})

One of the important requirements for traction application is high torque density. The torque density depends on the active weight of the motor. Among the three types of motor, Type I has the highest Torque per unit Active Weight.

$$T_{AW} = \frac{T_{\text{rated}}}{\text{Activeweight}} \quad (22)$$

where T_{rated} – Rated Torque in Nm.

4.5. Torque per unit active volume (T_{AV})

The smaller size of the machine results in compactness

of the size. The torque per active volume of the Type III motor is higher than that of the Type I motor but nearly twice that of type II motors.

$$T_{AV} = \frac{T_{rated}}{\text{Activevolume}} \quad (23)$$

4.6. Copper loss (P_c)

High copper loss results in poor efficiency and high operating cost. Copper loss of Type II and Type III is closer to each other but Type I has a higher copper loss.

$$P_c = I^2 R \quad (24)$$

where I – Current in amperes; R – resistance per phase in ohms.

4.7. Copper weight (W_c) and iron weight (W_i)

Copper weight is calculated from the cross-sectional area of the conductor, length of the conductor and mass density. The cost of the machine is much affected by the copper weight and Iron weight. Copper is much costlier than Iron. Hence reduction in copper weight leads to lesser cost for the machine. Type II and III have copper weights closer to each other but Type I has a higher copper weight. The iron weight of Type I is lower than that of the other two types.

5. Prototyping of type III configuration

The exploded view of the Type III configuration is shown in Figure 17. The Stator core is made by machining a toroidal core made of M-36 grade, 0.35 mm thickness silicon steel. The retaining disc of the rotor is made up of non-magnetic Epoxy Resin Laminate (ERL) to ensure the proper flow of flux and to eliminate eddy current. The rotor segments are made up of M-36 grade,

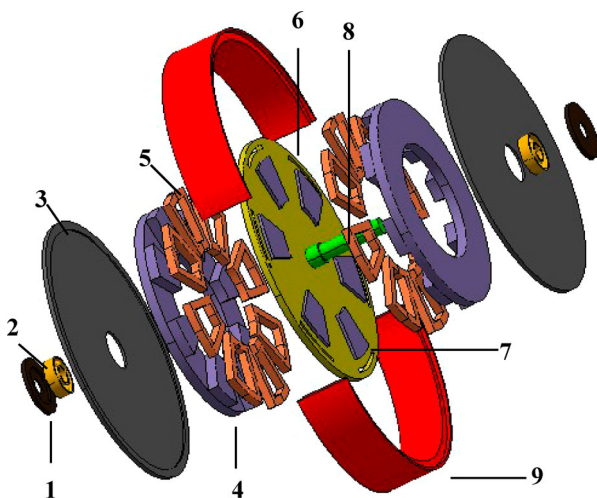


Figure 17. Exploded view of Type III configuration. 1. Bearing support plate, 2. Bearing, 3. End cover, 4. Stator, 5. Winding, 6. Retaining Disc of rotor, 7. Rotor pole, 8. Shaft, 9. Frame.

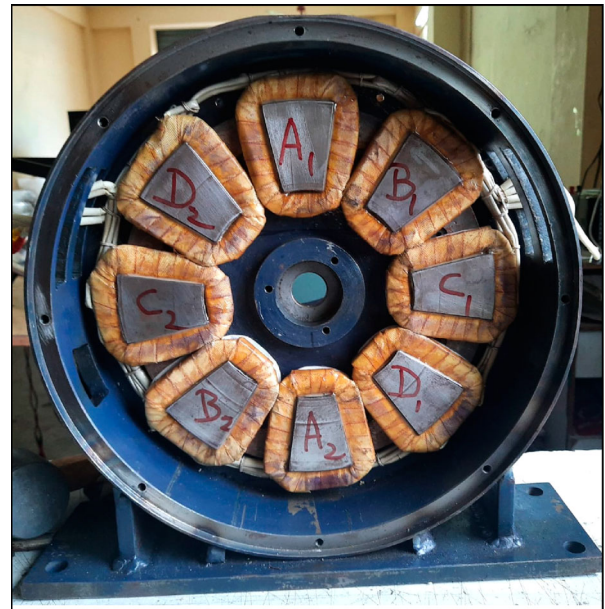


Figure 18. Wounded stator inside the motor frame.



Figure 19. Segmented rotor poles embedded in Epoxy Resin Laminate.

0.35 mm thickness silicon steel. The retaining disc is bolted to the shaft to avoid keyway and key arrangement. The wounded stator, embedded rotor segments in ERL and assembled prototype are shown in Figures 18–20. Table 4 shows the specification of the prototype.

6. Experimental validation

An experimental set-up to obtain static characteristics of the prototype is shown in Figure 21. The inductance of the motor is obtained at different rotor positions. The experimental procedure is a conventional method of calculating inductance from measured impedance and resistance. For a more accurate RMS value Tektronix MDO 3014 mixed domain oscilloscope is used to capture the voltage and current waveform. Figure



Figure 20. Assembled prototype.

Table 4. Specification of the fabricated motor.

Parameter	Value
The outer diameter of the stator (mm)	254
The inner diameter of the stator (mm)	145
Axial length (mm)	55
Stator pole arc (deg)	21
Rotor pole arc (deg)	26
Turns/phase	18
Air gap (mm)	0.5 mm
Peak rated current (A)	25
Core material	M-36 Steel

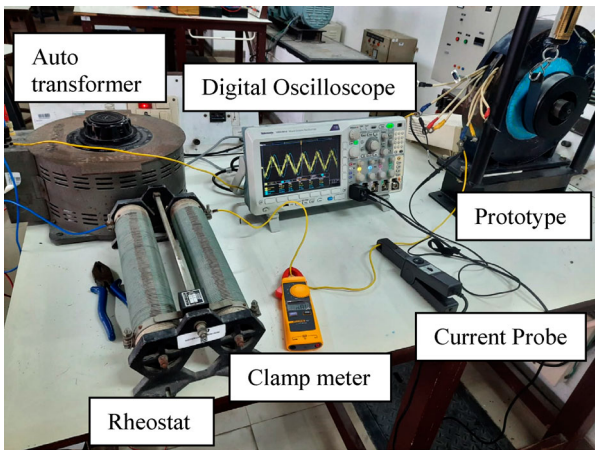


Figure 21. Experimental set-up.

22 shows the oscilloscope output at an aligned position. Figure 23 shows the inductance profile obtained through experiment and FEA.

7. Conclusion

Three different configurations of Switched Reluctance Motors suitable for EV applications are designed for

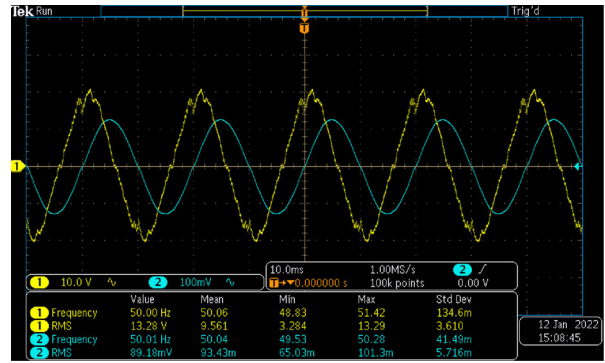


Figure 22. Voltage and current waveform at the aligned position.

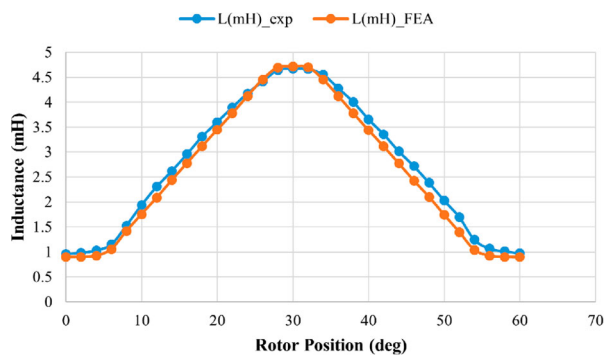


Figure 23. Inductance at different rotor positions.

Table 5. Comparison of the three types of configurations.

Parameter	Type I	Type II	Type III
Highest L_a/L_u ratio	X	X	✓
Least aligned inductance	✓	X	X
Least unaligned inductance	X	X	✓
Least torque ripple	X	X	✓
Least active weight	✓	X	X
Least copper loss	X	✓	X
Highest torque per unit active weight	✓	X	X
Highest torque per unit active volume	X	X	✓

a power rating of 1 hp. The electromagnetic analysis of the configurations is done using the Finite Element Analysis software, MagNet. The significant performance indices such as Torque ripple, Torque per unit active weight and Torque per unit active volume, and the design features such as Aligned inductance, Unaligned inductance, L_a/L_u ratio, Active weight and Copper loss of each configuration are compared to find the best configuration. From Table 5 it is evident that the Type II configuration fails to lead the other two configurations in most aspects. Though Type I configuration is superior in the aspects of Least active weight and Highest power per unit active weight, the difference from Type III is not significant. From the analysis it is concluded that Type III is the best configuration among the three chosen configurations for EV application. A prototype of the best configuration is made and experimental validation is done. An efficient control algorithm will yield better performance.

Disclosure statement

No potential conflict of interest was reported by the author(s).

Funding

This work was supported by Science and Engineering Research Board, Department of Science and Technology (DST), India [Grant Number EEQ/2017/000457].

ORCID

L. Ananda Padmanaban  <http://orcid.org/0000-0002-9440-8060>

References

- [1] Zan X, Xu G, Zhao T, et al. Multi-battery block module power converter for electric vehicle driven by switched reluctance motors. *IEEE Access*. 2021;9:140609–140618.
- [2] Yueying Z, Chuantian Y, Yuan Y, et al. Design and optimisation of an in-wheel switched reluctance motor for electric vehicles. *IET Intel Transport Syst*. 2019;13(1):175–182.
- [3] Jhunjhunwala A, Kaur P, Mutagekar S. Electric vehicles in India: a novel approach to scale electrification. *IEEE Electrification Mag*. 2018;6(4):40–47.
- [4] Whitehead A, Hilton C. In-wheel motors roll again. *IEEE Spectr*. 2018;55(7):24–29.
- [5] Profumo F, Zhang Z, Tenconi A. Axial flux machines drives: a new viable solution for electric cars. *IEEE Trans Ind Electron*. 1997;44(1):39–45.
- [6] Patel NR, Shah VA, Lokhande MM. A novel approach to the design and development of 12/15 radial field C-core switched reluctance motor for implementation in electric vehicle application. *IEEE Trans Veh Technol*. 2018;67(9):8031–8040.
- [7] Gan C, Wu J, Sun Q, et al. A review on machine topologies and control techniques for low-noise switched reluctance motors in electric vehicle applications. *IEEE Access*. 2018;6:31430–31443.
- [8] Ma J, Qu R, Li J. Optimal design of axial flux switched reluctance motor for electric vehicle application. In *International Conference on Electrical Machines and Systems*; 2014.
- [9] Lin J, Lambert T, Yang Y, et al. A novel axial flux switched reluctance motor with multi-level air gap geometry. In *IEEE Electrical Power and Energy Conference*; 2016.
- [10] Li C, Wang G, Li Y, et al. Robust adaptive neural network control for switched reluctance motor drives. *Automatika*. 2018;59(1):24–34.
- [11] Abdalmagid M, Sayed E, Bakr MH, et al. Geometry and topology optimization of switched reluctance machines: a review. *IEEE Access*. 2022;10:5141–5170.
- [12] Krishnan R, Abouzeid M, Mang X. A design procedure for axial field switched reluctance motors. In *Conference Record of the 1990 IEEE Industry Applications Society Annual Meeting*; 1990.
- [13] Pulle DWJ, Petersen IR. A unified approach to switched reluctance drive modeling: application to an axial flux (SRAF) motor. In *PESC 98 Record. 29th Annual IEEE Power Electronics Specialists Conference*; 1998.
- [14] Mao S-H, Tsai M-C. A novel switched reluctance motor with C-core stators. *IEEE Trans Magn*. 2005;41(12):4413–4420.
- [15] Labak A, Kar NC. A novel five-phase pancake shaped switched reluctance motor for hybrid electric vehicles. In *IEEE Vehicle Power and Propulsion Conference*; 2009.
- [16] Madhavan R, Fernandes BG. A novel axial flux segmented SRM for electric vehicle application. In *The XIX International Conference on Electrical Machines – ICEM 2010*; 2010.
- [17] Madhavan R, Fernandes BG. Comparative analysis of axial flux SRM topologies for electric vehicle application. In *IEEE International Conference on Power Electronics, Drives and Energy Systems*; 2012.
- [18] Sengupta M, Ahmad SS, Mukherjee D. Experimental investigations on a novel laboratory prototype of axial flux switched reluctance motor. In *IEEE International Conference on Power Electronics, Drives and Energy Systems (PEDES)*; 2012.
- [19] Kellerer T, Radler O, Sattel T, et al. “Axial type switched reluctance motor of soft magnetic composite. In *Innovative Small Drives and Micro-Motor Systems*; 9. *GMM/ETG Symposium*; 2013.
- [20] Ma J, Qu R, Li J. Optimal design of axial flux switched reluctance motor for electric vehicle application. In *International Conference on Electrical Machines and Systems (ICEMS)*; 2014.
- [21] Kermanipour MJ, Ganji B. Modification in geometric structure of double-sided axial flux switched reluctance motor for mitigating torque ripple. *Can J Electr Comput Eng*. 2015;38(4):318–322.
- [22] Pan Z, Song S, Ma R. A novel axial flux switched reluctance machine with segmented stator and rotor. In *International Conference on Electrical Machines and Systems (ICEMS)*; 2017.